Hydrodynamics of sediment threshold

Sk Zeeshan Ali and Subhasish Dey

Citation: Phys. Fluids **28**, 075103 (2016); doi: 10.1063/1.4955103
View online: http://dx.doi.org/10.1063/1.4955103
View Table of Contents: http://aip.scitation.org/toc/phf/28/7
Published by the American Institute of Physics

PHYSICS OF FLUIDS **28**, 075103 (2016)

Hydrodynamics of sediment threshold

Sk Zeeshan Ali[a)] and Subhasish Dey
Department of Civil Engineering, Indian Institute of Technology, Kharagpur 721302, West Bengal, India

(Received 21 March 2016; accepted 20 June 2016; published online 6 July 2016)

A novel hydrodynamic model for the threshold of cohesionless sediment particle motion under a steady unidirectional streamflow is presented. The hydrodynamic forces (drag and lift) acting on a solitary sediment particle resting over a closely packed bed formed by the identical sediment particles are the primary motivating forces. The drag force comprises of the form drag and form induced drag. The lift force includes the Saffman lift, Magnus lift, centrifugal lift, and turbulent lift. The points of action of the force system are appropriately obtained, for the first time, from the basics of micro-mechanics. The sediment threshold is envisioned as the rolling mode, which is the plausible mode to initiate a particle motion on the bed. The moment balance of the force system on the solitary particle about the pivoting point of rolling yields the governing equation. The conditions of sediment threshold under the hydraulically smooth, transitional, and rough flow regimes are examined. The effects of velocity fluctuations are addressed by applying the statistical theory of turbulence. This study shows that for a hindrance coefficient of 0.3, the threshold curve (threshold Shields parameter versus shear Reynolds number) has an excellent agreement with the experimental data of uniform sediments. However, most of the experimental data are bounded by the upper and lower limiting threshold curves, corresponding to the hindrance coefficients of 0.2 and 0.4, respectively. The threshold curve of this study is compared with those of previous researchers. The present model also agrees satisfactorily with the experimental data of nonuniform sediments. *Published by AIP Publishing.* [http://dx.doi.org/10.1063/1.4955103]

I. INTRODUCTION

Sediment threshold is defined as the hydrodynamic condition for which the sediment particles on the surface of a sediment bed are on the verge of motion. Since the past years, this topic has attracted the attention of several investigators in order to understand the rheology of the transport of solid sediment particles through laboratory experiments and field measurements.[1–4] In general, it is ascertained making use of the famous Shields diagram that represents a curve of threshold Shields parameter Θ_c versus threshold shear Reynolds number R_{*c} called the *threshold curve.*[5] The Shields diagram is extensively used to determine the threshold bed shear stress for a given sediment size. Since the Shields diagram was prepared in 1936 using the limited experimental data, a slight departure of the threshold curve from the subsequent experimental data was reported in the literature.[6–8] Important studies on sediment threshold were thoroughly reviewed by several investigators.[7,9–12]

The concept of threshold bed shear stress was applied by various researchers to describe the sediment threshold phenomenon.[12] This concept is based on the principle of force balance between the destabilizing hydrodynamic forces (drag and lift) and the stabilizing forces due to the submerged weight and the inter-particle friction. In some studies, the idea of moment balance of the force system

[a)]Author to whom correspondence should be addressed. Electronic mail: skzeeshanali@iitkgp.ac.in

about the pivoting point was applied to determine the condition of sediment threshold.[13–19] The inclusion of turbulence in the force balance model was due to White,[20] who introduced a turbulence factor in his analysis to account for the instantaneous bed shear stress. Since then, the effects of turbulence on sediment threshold were successfully addressed in several studies.[17–19,21–28] Although the drag force is the predominant hydrodynamic force being responsible for the sediment threshold, the lift force can also play an important role to initiate the sediment motion. Several researchers considered the lift force arising from the steep velocity gradient in the vicinity of the bed,[29,30] the slip-spinning of particle,[14,15] and the turbulent velocity fluctuations.[18,31,32] The effects of friction angle, exposure, sorting, and hiding of sediment particles on threshold bed shear stress were studied by Wiberg and Smith,[30] Fenton and Abbott,[33] Kirchner *et al.*,[34] Komar and Carling,[35] Johnston *et al.*,[36] and Luckner.[37] Further, the effects of bed slope on the threshold bed shear stress were evaluated by Ikeda,[32] Fernandez Luque and van Beek,[38] Chiew and Parker,[39] Armanini and Gregoretti,[40] and Lamb *et al.*[41] The salient features of the trajectories and the different states of motion of sediment particles were reported by Francis,[42] Abbott and Francis,[43] White and Schulz,[44] and Ancey *et al.*[45] Munro[46] experimentally investigated the interaction between the vortex ring and the sloped sediment layer under a threshold condition. The threshold Shields parameters Θ_c measured from the experiments were compared with those obtained from the mathematical model stemming from the principle of force balance. Agudo *et al.*[47] experimentally studied the effects of neighboring bed particles on the initiation of particle motion under a laminar flow condition. They found that rolling is the primary mechanism of the initiation of spherical particle motion. The role of near-bed pressure forces on sediment threshold was reported by Vollmer and Kleinhans,[18] Amir *et al.*,[48] and Celik *et al.*[49] The pressure forces are of primary importance to the sediment threshold phenomenon because the pressure differences across the sediment particle in the streamflow direction and perpendicular to the streamflow direction contribute to the drag and lift forces, respectively, exerted on the sediment particle.

The major drawback of most of the previous force balance models is that the point of action of the force system was not determined from the basics of the mechanics. In addition, the forces acting on a solitary particle were analyzed using a two-dimensional (2D) approach.[14,17,24–26,28,30] Although Dey[15] provided an analysis of sediment threshold treating a three-dimensional (3D) configuration of the bed particles, the effects of turbulent fluctuations were ignored. The limitations of the previous studies are more specifically delineated in Appendix A. In this study, we present a novel mathematical model to determine the threshold Shields parameter for the initiation of cohesionless sediment particles under a steady unidirectional flow over a sediment bed. We consider the sediment particles as discrete spherical particles. The mode of sediment threshold is envisaged as the rolling mode, which is the most plausible mode to initiate a particle motion on the sediment bed. The moment of the force system about the pivoting point constitutes the governing equation. The analysis starts with the proper configuration of bed sediment particles in a 3D configuration. The hydrodynamic forces (drag and lift) acting on a solitary particle resting over three closely packed bed particles are analyzed. The drag force is due to the form drag and form induced drag. On the other hand, the lift force is due to the shear (Saffman lift), spinning motion (Magnus lift), rolling over bed particles (centrifugal lift), and advective vertical acceleration (turbulent lift).[12] An in-depth analysis is pursued, for the first time, from the basics of the micro-mechanics, addressing the typical points of action of the force system. Three different velocity laws are considered to examine the sediment threshold under hydraulically smooth, transitional, and rough flow regimes. The effects of turbulent fluctuations are incorporated by applying the statistical theory of turbulence.[50,51]

The rest of the paper is organized as follows: the mathematical formulation is developed in Sec. II. The computational steps are described in Sec. III. The model results and discussion are presented in Sec. IV. Finally, the conclusions are drawn in Sec. V.

II. MATHEMATICAL FORMULATION

A. Configuration of bed sediment particles

To start the mathematical formulation, a consideration of the proper configuration of bed sediment particles is an essential prerequisite because the mobility of individual particles depends on the

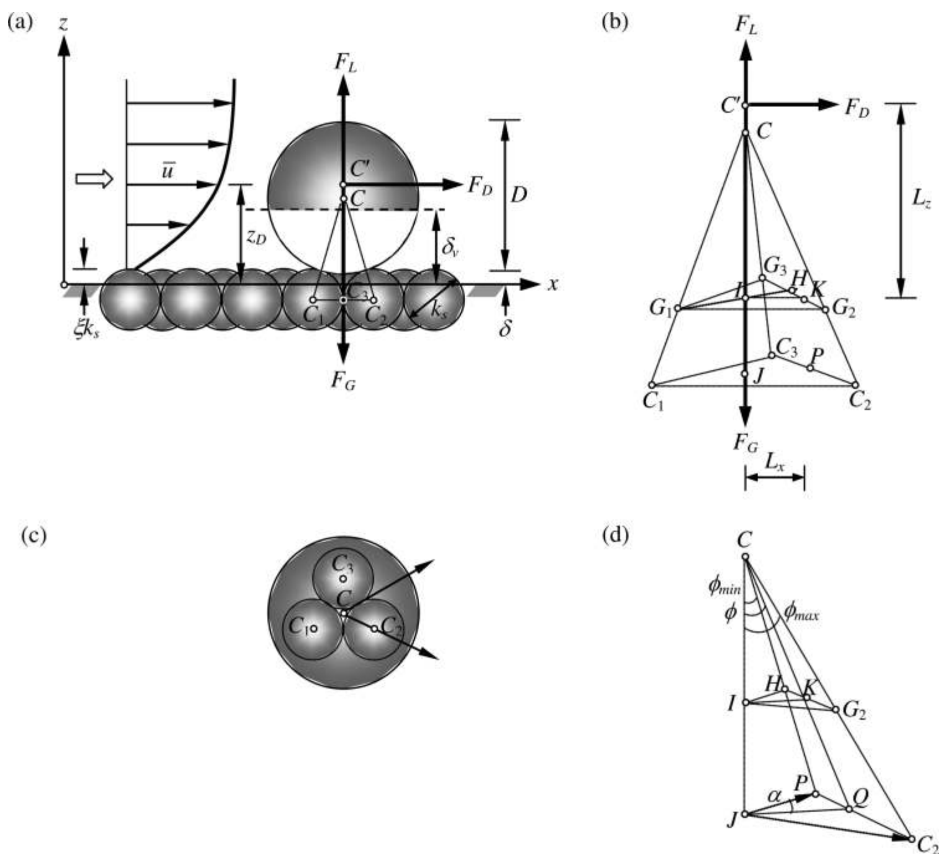

FIG. 1. Schematic of (a) the configuration of bed sediment particles and the force system in the xz-plane (C_1, C_2, and C_3 lie on the plane parallel to the xy-plane), (b) the tetrahedron $CC_1C_2C_3$, (c) the plan view of bed sediment particles (two arrowheads represent the direction of rolling for two extreme cases), and (d) the tetrahedron CJC_2P and the maximum, minimum, and mean pivoting angles.

configuration of bed particles. It is worth mentioning that the consideration of the configuration of bed sediment particles in a sediment bed for more natural condition does not guarantee an initial stability to the solitary particle. Further, it makes the analysis uncertain since the packing of the bed sediment particles under natural conditions is numerous. Therefore, the configuration of bed sediment particles is envisioned as a spherical solitary sediment particle of diameter D resting over a closely packed bed formed by three identically spherical bed particles of diameter k_s (see Fig. 1(a)). The coordinate system is depicted in Fig. 1(a). Figure 1(a) shows a generalized view as $D > k_s$; however, other cases ($D \leq k_s$) are also possible. The reason to consider such a configuration is that it essentially provides an initial stability of the solitary particle before the dislodgement in rolling mode from its initial position under the action of hydrodynamic forces. Similar configuration of bed sediment particles was considered by Coleman,[13] Dey,[15] Miller and Byrne,[52] and others. A tetrahedron $CC_1C_2C_3$ is formed by connecting the centers of the solitary and the bed particles (see Fig. 1(a)). The enlarged view of the tetrahedron $CC_1C_2C_3$ is further depicted in Fig. 1(b). It may be noted that C_1, C_2, and C_3 lie on the plane parallel to xy-plane. In Fig. 1(b), G_1, G_2, and G_3 are the points of contact. The points I and J are the projections of point C on $G_1G_2G_3$ and $C_1C_2C_3$ planes, respectively, and the points H and P are the midpoints of lengths $r_{G_2G_3}$ and $r_{C_2C_3}$, respectively, where the symbol r_{AB} denotes the distance between two points A and B.

The x-axis or the virtual bed level (that is, $z = 0$) is considered at a normal distance ξk_s below the summit of the bed particles. Here, ξ is a factor being smaller than unity. Let the lowermost point of the solitary particle be located at a distance δ from the virtual bed level. Then,

$\delta = \xi k_s - 0.5(D + k_s) + r_{CJ}$. From the geometry, the r_{CJ} is

$$r_{CJ} = (r_{CC_2}^2 - r_{C_2J}^2)^{0.5} = \left[\left(\frac{D+k_s}{2}\right)^2 - \left(\frac{k_s}{\sqrt{3}}\right)^2\right]^{0.5} = \frac{1}{2\sqrt{3}}(3D^2 + 6Dk_s - k_s^2)^{0.5}. \tag{2.1}$$

Therefore, the δ in nondimensional form is given by

$$\delta^+ \left(= \frac{\delta}{D}\right) = \xi k_s^+ - 0.5(1 + k_s^+) + \frac{1}{2\sqrt{3}}(3 + 6k_s^+ - k_s^{+2})^{0.5}, \tag{2.2}$$

where k_s^+ is k_s/D.

Figure 1(c) shows the plan view of bed sediment particles. The principal mode of sediment threshold is the rolling mode, since the sediment threshold in rolling mode is most likely for spherical particles.[15,17,18,24,47,52–55] In the rolling mode, the solitary particle has two bounds depending on the orientation of the bed particles with respect to the streamflow direction. The particle can roll either over the summit of a single bed particle or through the flank of the two contiguous bed particles as depicted in Fig. 1(c) by the two arrowheads. In the former case, the solitary particle rolls over the summit of a single bed particle in the direction JC_2 making the pivoting angle a maximum (angle $C_2CJ = \phi_{max}$) (see Fig. 1(d)). On the other hand, in the latter case, the solitary particle rolls through the flank of two bed particles in the direction JP making the pivoting angle a minimum (angle $PCJ = \phi_{min}$) (see Fig. 1(d)). From the geometry, the values of ϕ_{max} and ϕ_{min} are thus obtained as

$$\phi_{max} = \tan^{-1}\frac{r_{C_2J}}{r_{CJ}} = \tan^{-1}\left[\frac{2k_s^+}{(3 + 6k_s^+ - k_s^{+2})^{0.5}}\right], \tag{2.3}$$

$$\phi_{min} = \tan^{-1}\frac{r_{JP}}{r_{CJ}} = \tan^{-1}\left[\frac{k_s^+}{(3 + 6k_s^+ - k_s^{+2})^{0.5}}\right]. \tag{2.4}$$

Let the most likely route followed by the solitary particle during the rolling mode be in the direction JQ, where $JQ \in [JP, JC_2]$ (see Fig. 1(d)). For such a situation, the pivoting angle QCJ is $\phi \in [\phi_{min}, \phi_{max}]$. Considering an angle α (see Fig. 1(d)), the mean value of r_{JQ} is obtained as

$$r_{JQ} = \frac{1}{\pi/3}\int_0^{\pi/3} r_{JQ}\mathrm{d}\alpha = \frac{3}{\pi}\int_0^{\pi/3} r_{JP}\sec\alpha\,\mathrm{d}\alpha = \frac{3}{\pi} r_{JP}\ln(2 + \sqrt{3}). \tag{2.5}$$

Therefore, the mean value of pivoting angle ϕ_m is

$$\phi_m = \tan^{-1}\frac{r_{JQ}}{r_{CJ}} = \tan^{-1}\left[\frac{3}{\pi}\ln(2 + \sqrt{3})\frac{r_{JP}}{r_{CJ}}\right]. \tag{2.6}$$

Using Eq. (2.4), Eq. (2.6) reduces to

$$\phi_m = \tan^{-1}\left[\frac{3}{\pi}\ln(2 + \sqrt{3})\frac{k_s^+}{(3 + 6k_s^+ - k_s^{+2})^{0.5}}\right]. \tag{2.7}$$

It follows that for a given k_s^+, the ϕ_m can be obtained from Eq. (2.7) or *vice versa*. Therefore, the tetrahedral configuration of sediment particles allows us to link between the ratio of bed particle diameter to solitary particle diameter and the mean pivoting angle, which is a physical quantity and feasible to determine.

B. Analysis of force system

The force system acting on the solitary particle is shown in Fig. 1(a). We split the hydrodynamic force experienced by the solitary particle into two components. The drag force F_D acts in the streamflow direction (x-direction) and the lift force F_L acts normal (z-direction) to the streamflow direction. Moreover, the submerged weight F_G of the particle acts through its center of gravity in the negative z-direction. The submerged weight of the solitary particle is

$$F_G = \frac{\pi}{6}D^3\Delta\rho_f g, \tag{2.8}$$

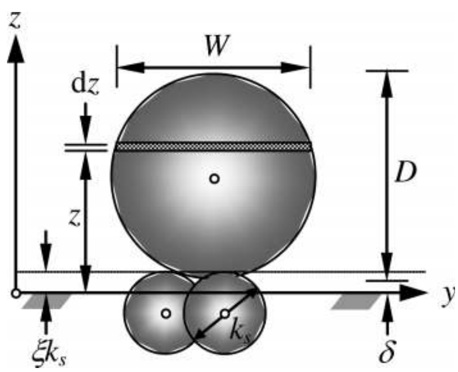

FIG. 2. Schematic of flow velocity received by the frontal area of the solitary particle in the yz-plane.

where Δ is the submerged relative density $[= (\rho_s - \rho_f)/\rho_f]$, ρ_s is the sediment mass density, ρ_f is the fluid mass density, and g is the gravitational acceleration.

The local instantaneous velocity components (u, w) in (x, z) are decomposed as $u = \bar{u} + u'$ and $w = \bar{w} + w'$, where over-bar denotes the time-averaged quantity and prime denotes the fluctuations with respect to time-averaged quantity. Since the summits of the bed particles upstream of the solitary particle encroach the flow beneath the $z = \xi k_s$ plane, the frontal area of the solitary particle exposed to the flow is considered as the projected area of the portion of the sphere above that plane[17,34] (see Fig. 2). Considering an elementary strip of length W in the yz-plane across the solitary particle at any vertical distance z, the frontal area $\mathrm{d}A$ of the elementary strip is $\mathrm{d}A = W\mathrm{d}z$. From the geometry, $W = 2[(z-\delta)(D+\delta-z)]^{0.5}$. Therefore, $\mathrm{d}A = 2[(z-\delta)(D+\delta-z)]^{0.5}\mathrm{d}z$. Integrating $\mathrm{d}A$ within limits $z = D+\delta$ and any vertical distance $z \in (\xi k_s, D+\delta)$, the frontal area A_z, representing the projected area bounded within $z = D+\delta$ and any vertical distance $z \in (\xi k_s, D+\delta)$, is obtained as

$$A_z = 0.25D^2\{\pi - \cos^{-1}(D+2\delta-2z) + 2(D+2\delta-2z)[(D+\delta-z)(z-\delta)]^{0.5}\}. \tag{2.9}$$

The components of drag force F_D in the xz-plane and lift force F_L in the yz-plane are depicted in Fig. 3 for two cases. In the former case (see Fig. 3(a)), the center of the solitary particle is submerged within the viscous sublayer thickness δ_v, that is, $\delta_v \in [0.5D+\delta, D+\delta]$. On the other hand, in the latter case (see Fig. 3(b)), the center of the solitary particle lies above the viscous sublayer thickness δ_v, that is, $\delta_v \in [0, 0.5D+\delta]$.

The time-averaged drag force F_D comprises of the form drag F_{D1} and the form induced drag F_{D2} due to streamwise pressure gradient (see Fig. 3). Thus, the total drag force is

$$F_D = F_{D1} + F_{D2}. \tag{2.10}$$

The form drag F_{D1} is expressed as (see Fig. 3)

$$F_{D1} = 0.5C_D\rho_f \int_{\xi k_s}^{D+\delta} \bar{u}^2 \mathrm{d}A, \tag{2.11}$$

where C_D is the drag coefficient. The point of action of F_{D1} is at (see Fig. 3)

$$z_{D1} = \xi k_s + \frac{\int_{\xi k_s}^{D+\delta} \bar{u}^2 z \mathrm{d}A}{\int_{\xi k_s}^{D+\delta} \bar{u}^2 \mathrm{d}A} = \xi k_s + \frac{\int_{\xi k_s}^{D+\delta} \bar{u}^2 z[(z-\delta)(D+\delta-z)]^{0.5}\,\mathrm{d}z}{\int_{\xi k_s}^{D+\delta} \bar{u}^2[(z-\delta)(D+\delta-z)]^{0.5}\,\mathrm{d}z}. \tag{2.12}$$

The form induced drag F_{D2} is expressed as (see Fig. 3)

$$F_{D2} = -\left(\frac{\partial \bar{p}}{\partial x}\right)_{z=z_{D2}} TA_{z=\delta_v}, \tag{2.13}$$

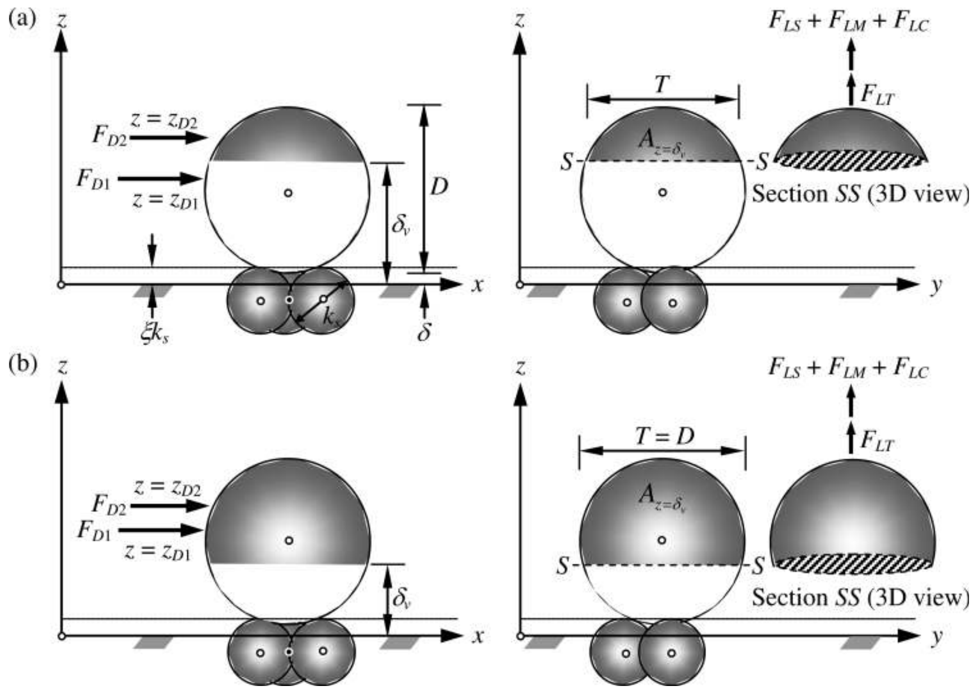

FIG. 3. Schematic of the components of drag force F_D (form drag F_{D1} and form induced drag F_{D2}) in the *xz*-plane and lift force F_L (Saffman lift F_{LS}, Magnus lift F_{LM}, centrifugal lift F_{LC}, and turbulent lift F_{LT}) in the *yz*-plane for (a) $\delta_v \in [0.5D+\delta, D+\delta]$ and (b) $\delta_v \in [0, 0.5D+\delta]$.

where $\bar{p}$ is the time-averaged pressure intensity, z_{D2} is the point of action of F_{D2}, and T is the width of an elementary strip in the *yz*-plane across the solitary particle at $z = \delta_v$. The width of the elementary strip T is expressed as (see Fig. 3)

$$T = 2[(\delta_v - \delta)(D + \delta - \delta_v)]^{0.5} \ \forall\ \delta_v \in [0.5D + \delta, D + \delta], \tag{2.14}$$

$$T = D \ \forall\ \delta_v \in (0, 0.5D + \delta). \tag{2.15}$$

The point of action of F_{D2} is at (see Fig. 3)

$$z_{D2} = 0.5(D + \delta + \delta_v) \ \forall\ \delta_v \in [\xi k_s, D + \delta], \tag{2.16}$$

$$z_{D2} = 0.5(D + \delta + \xi k_s) \ \forall\ \delta_v \in (0, \xi k_s). \tag{2.17}$$

To find the time-averaged pressure gradients in x- and z-direction, we assume that the time-averaged pressure gradients are free from the viscous effects in order to simplify the mathematical treatment. Thus, the Euler equations in x- and z-direction produce

$$-\frac{\partial \bar{p}}{\partial x} = \rho_f \overline{\frac{\mathrm{D}u}{\mathrm{D}t}}, \tag{2.18}$$

$$-\frac{\partial \bar{p}}{\partial z} = \rho_f \overline{\frac{\mathrm{D}w}{\mathrm{D}t}}, \tag{2.19}$$

where $\mathrm{D}u/\mathrm{D}t$ and $\mathrm{D}w/\mathrm{D}t$ refer to the total acceleration components in (x, z).

Thus, using Eqs. (2.11), (2.13), and (2.18), Eq. (2.10) reduces to

$$F_D = C_D \rho_f \int_{\xi k_s}^{D+\delta} \bar{u}^2[(z - \delta)(D + \delta - z)]^{0.5} \mathrm{d}z + \rho_f \left(\overline{\frac{\mathrm{D}u}{\mathrm{D}t}} \right)_{z=z_{D2}} T A_{z=\delta_v}. \tag{2.20}$$

Therefore, the F_D in nondimensional form is

$$F_D^+\left(=\frac{F_D}{\rho_f u_*^2 D^2}\right) = C_D \int_{\xi k_s^+}^{1+\delta^+} \bar{u}^{+2}[(z_0^+ - \delta^+)(1+\delta^+ - z_0^+)]^{0.5}\mathrm{d}z_0^+ + \left(\overline{\frac{\mathrm{D}u^+}{\mathrm{D}t^+}}\right)_{z_0^+=z_{D2}^+} T^+ A^+_{z_0^+=\delta_v^+}, \tag{2.21}$$

where $\bar{u}^+$ is $\bar{u}/u_*$, z_0^+ is z/D, δ_v^+ is δ_v/D, u^+ is u/u_*, u_* is the shear velocity, t^+ is tu_*/D, T^+ is T/D, and A^+ is A/D^2.

Analyzing the data of Coleman,[13] the drag coefficient C_D can be expressed as a function of shear Reynolds number R_* ($= u_* k_s/\upsilon$, where υ is the kinematic viscosity) in the following form:[18]

$$\begin{aligned} C_D(R_* \le 5) &= \frac{25}{R_*},\\ C_D(5 < R_* \le 5\times 10^4) &= 0.55 + \frac{37}{R_*^{1.2}} - \frac{3.5}{R_*^{0.9}},\\ C_D(R_* > 5\times 10^4) &= 0.25. \end{aligned} \tag{2.22}$$

The F_D acting at the point C' (see Figs. 1(a) and 1(b)) is at an elevation

$$z_D = \frac{\sum_{i=1}^{2} F_{Di} z_{Di}}{F_D}. \tag{2.23}$$

For a steady flow, the local acceleration terms disappear yielding $\mathrm{D}u/\mathrm{D}t = u(\partial u/\partial x) + w(\partial u/\partial z)$ and $\mathrm{D}w/\mathrm{D}t = u(\partial w/\partial x) + w(\partial w/\partial z)$. Substituting $u = \bar{u} + u'$ and $w = \bar{w} + w'$ in $\mathrm{D}u/\mathrm{D}t$ and $\mathrm{D}w/\mathrm{D}t$ and performing the time-averaging yield

$$\overline{\frac{\mathrm{D}u}{\mathrm{D}t}} = \overline{(\bar{u}+u')\frac{\partial(\bar{u}+u')}{\partial x}} + \overline{(\bar{w}+w')\frac{\partial(\bar{u}+u')}{\partial z}}, \tag{2.24}$$

$$\overline{\frac{\mathrm{D}w}{\mathrm{D}t}} = \overline{(\bar{u}+u')\frac{\partial(\bar{w}+w')}{\partial x}} + \overline{(\bar{w}+w')\frac{\partial(\bar{w}+w')}{\partial z}}. \tag{2.25}$$

For a unidirectional (streamwise, that is, in x-direction) and uniform streamflow over a sediment bed, $\bar{u} = \bar{u}(z)$, $\bar{w} = 0$ (that is, $w = w'$),[56] and $\partial\bar{u}/\partial x = 0$. Therefore, Eqs. (2.24) and (2.25) reduce to

$$\overline{\frac{\mathrm{D}u}{\mathrm{D}t}} = \overline{u'\frac{\partial u'}{\partial x}} + \overline{w'\frac{\partial u'}{\partial z}}, \tag{2.26}$$

$$\overline{\frac{\mathrm{D}w}{\mathrm{D}t}} = \overline{u'\frac{\partial w'}{\partial x}} + \overline{w'\frac{\partial w'}{\partial z}}. \tag{2.27}$$

Since there are no data providing the correlation coefficients for $u'(\partial u'/\partial x)$, $w'(\partial u'/\partial z)$, $u'(\partial w'/\partial x)$, and $w'(\partial w'/\partial z)$, we can adopt the root mean squares of them.[57] Therefore, we obtain

$$\overline{\frac{\mathrm{D}u}{\mathrm{D}t}} = \sqrt{\overline{u'^2}}\sqrt{\overline{\left(\frac{\partial u'}{\partial x}\right)^2}} + \sqrt{\overline{w'^2}}\sqrt{\overline{\left(\frac{\partial u'}{\partial z}\right)^2}}, \tag{2.28}$$

$$\overline{\frac{\mathrm{D}w}{\mathrm{D}t}} = \sqrt{\overline{u'^2}}\sqrt{\overline{\left(\frac{\partial w'}{\partial x}\right)^2}} + \sqrt{\overline{w'^2}}\sqrt{\overline{\left(\frac{\partial w'}{\partial z}\right)^2}}. \tag{2.29}$$

By applying the statistical theory of turbulence,[50,51] we obtain

$$\overline{\left(\frac{\partial u'}{\partial x}\right)^2} = \frac{\overline{u'^2}}{\lambda^2}, \tag{2.30}$$

$$\overline{\left(\frac{\partial u'}{\partial z}\right)^2} = \frac{2\overline{u'^2}}{\lambda^2} + \frac{1}{4\overline{u'^2}}\left(\frac{\partial\overline{u'^2}}{\partial z}\right)^2, \tag{2.31}$$

$$\overline{\left(\frac{\partial w'}{\partial x}\right)^2} = \frac{2\overline{w'^2}}{\lambda^2}, \tag{2.32}$$

where λ is the Taylor micro-scale.

Substituting Eqs. (2.30)–(2.32) in Eqs. (2.28) and (2.29) yields

$$\overline{\frac{\mathrm{D}u^+}{\mathrm{D}t^+}} = \frac{1}{k_s^+}\left\{\frac{\sigma_u^{+2}}{\lambda^+} + \sigma_w^+\left[\frac{2\sigma_u^{+2}}{\lambda^{+2}} + \left(\frac{\partial \sigma_u^+}{\partial z^+}\right)^2\right]^{0.5}\right\}, \tag{2.33}$$

$$\overline{\frac{\mathrm{D}w^+}{\mathrm{D}t^+}} = \frac{1}{k_s^+}\left[\frac{\sqrt{2}\sigma_u^+\sigma_w^+}{\lambda^+} + \sigma_w^+\frac{\partial \sigma_w^+}{\partial z^+}\right], \tag{2.34}$$

where w^+ is w/u_*, σ_u^+ is σ_u/u_*, σ_u is the turbulence intensity in x-direction $[= (\overline{u'u'})^{0.5}]$, σ_w^+ is σ_w/u_*, σ_w is the turbulence intensity in z-direction $[= (\overline{w'w'})^{0.5}]$, z^+ is z/k_s, and λ^+ is λ/k_s.

The σ_u in nondimensional form is expressed as follows:[25]

$$\sigma_u^+ = 0.31z^+R_*\exp(-0.1z^+R_*) + 1.8\exp(-0.88\varpi^{-1})[1 - \exp(-0.1z^+R_*)], \tag{2.35}$$

where ϖ is the relative submergence $(= h/k_s)$ and h is the flow depth. The effects of the relative submergence ϖ on turbulence intensity are significant only for the shallow streamflow.[25,41] However, for natural streams, the ϖ is relatively large and hence has a trivial effect on σ_u-distribution. Equation (2.35) shows that the σ_u^+ is practically independent of ϖ for $\varpi \geq 100$.

The σ_w in nondimensional form is expressed as follows:[58,59]

$$\sigma_w^+ = 0.5\sigma_u^+. \tag{2.36}$$

To find λ^+, as it appears in the right hand side of Eqs. (2.33) and (2.34), we proceed as follows. The turbulent kinetic energy (TKE) dissipation rate ε is expressed as[60]

$$\varepsilon = \frac{0.691}{h^{0.5}}\frac{\sigma_u^3}{z^{0.5}}. \tag{2.37}$$

The Taylor micro-scale λ can be related to the TKE dissipation rate ε as[50,60]

$$\lambda = \left(15\upsilon\frac{\sigma_u^2}{\varepsilon}\right)^{0.5}. \tag{2.38}$$

Substituting Eq. (2.37) in Eq. (2.38) yields

$$\lambda^+ = \lambda_0^+ + \left(\frac{21.71}{R_*\varpi^{1.5}\sigma_u^+}\right)^{0.5} z^{+0.25}, \tag{2.39}$$

where λ_0^+ is λ_0/k_s and λ_0 is the amount of increase in size of the eddies depending on the bed roughness.[31,51]

The hydrodynamic lift force F_L is constituted by the Saffman lift F_{LS}, the Magnus lift F_{LM}, the centrifugal lift F_{LC}, and the turbulent lift F_{LT} (see Fig. 3). Thus, the total lift force is $F_L = F_{LS} + F_{LM} + F_{LC} + F_{LT}$.

The Saffman lift[61,62] on a particle arises when the particle is placed in a shear flow, which has a gradient in velocity distribution. The Saffman lift originates from the inertia effects in the shear flow around the particle. It is expressed as

$$F_{LS} = C_L\rho_f D^2 V\left(\upsilon\frac{\partial \bar{u}}{\partial z}\right)^{0.5}, \tag{2.40}$$

where C_L is the Saffman lift coefficient and V is the velocity of fluid at an elevation of the center of the solitary particle. In this study, we consider $C_L = 0.85C_D$.[63] The F_{LS} in nondimensional form is

$$F_{LS}^+\left(= \frac{F_{LS}}{\rho_f u_*^2 D^2}\right) = C_L V^+\left(\frac{k_s^+}{R_*}\frac{\partial \bar{u}^+}{\partial z_0^+}\right)^{0.5}, \tag{2.41}$$

where V^+ is V/u_*.

As the shear Reynolds numbers R_* gradually increases, the solitary particle starts rotating into the groove, formed by the three closely packed bed particles, just before dislodging from its initial position.[14,15] The rotation of the solitary particle is attributed to the steep velocity gradient $\partial\bar{u}/\partial z$ in the vicinity of the bed due to the substantial velocity gradient between the lowermost point ($z = \delta$) and the uppermost point ($z = D + \delta$) of the solitary particle. Thus, a turning moment is created due to a larger hydrodynamic force experienced by the upper portion of the particle than that by the lower portion of the particle. The lift force caused by the particle rotation, known as the Magnus lift,[64] is expressed as

$$F_{LM} = \rho_f D^3 \bar{u}_m \varOmega_m, \tag{2.42}$$

where $\bar{u}_m$ is the mean velocity received by the solitary particle, $\varOmega_m$ ($= 0.5\varOmega_{max}$) is the mean angular velocity of the solitary particle, and $\varOmega_{max} = 0.5(\partial\bar{u}/\partial z)$. The F_{LM} in nondimensional form is

$$F^+_{LM}\left(= \frac{F_{LM}}{\rho_f u_*^2 D^2}\right) = 0.25\bar{u}^+_m \frac{\partial\bar{u}^+}{\partial z^+_0}, \tag{2.43}$$

where $\bar{u}^+_m$ is $\bar{u}_m/u_*$.

The curvilinear motion of the solitary particle over the bed particles induces the centrifugal lift,[14] which is expressed as

$$F_{LC} = \frac{\pi D^3}{6}(\rho_s + \alpha_m\rho_f)\frac{(\varOmega_m D)^2}{4\mathfrak{R}}\cos\phi_m = \frac{\pi D^5}{384\mathfrak{R}}(\rho_s + \alpha_m\rho_f)\left(\frac{\partial\bar{u}}{\partial z}\right)^2\cos\phi_m, \tag{2.44}$$

where α_m is the added mass coefficient and $\mathfrak{R}$ is the radius of curvature of the locus of the moving solitary particle over the bed particles. The significance of an added fluid mass is the inertia added to a system. An accelerating or decelerating particle is to move some volume of surrounding fluid, as it moves through it. The value $\alpha_m = 0.5$ is used here as was considered by van Rijn.[65] The $\mathfrak{R}$ is considered as the length r_{CQ} (see Fig. 1(d)). Thus,

$$\mathfrak{R} = r_{CQ} = (r^2_{CJ} + r^2_{JQ})^{0.5} = \frac{1}{2\sqrt{3}}\left[(3D^2 + 6Dk_s - k_s^2) + \frac{9k_s^2}{\pi^2}\ln^2(2+\sqrt{3})\right]^{0.5}. \tag{2.45}$$

The F_{LC} in nondimensional form is

$$F^+_{LC}\left(= \frac{F_{LC}}{\rho_f u_*^2 D^2}\right) = \frac{\pi}{384\mathfrak{R}^+}(1 + \alpha_m + \varDelta)\left(\frac{\partial\bar{u}^+}{\partial z^+_0}\right)^2\cos\phi_m, \tag{2.46}$$

where $\mathfrak{R}^+$ is $\mathfrak{R}/D$.

The turbulent lift is developed due to the pressure gradient along the vertical, which can be correlated with the total acceleration component in the vertical direction (see Eq. (2.19)). To analyze the turbulent lift, we take a section *SS* of the solitary particle perpendicular to the *yz*-plane (see Fig. 3). The 3D view of the spherical cap is depicted in Fig. 3. The diameter of the base of the spherical cap is T (as defined in Eqs. (2.14) and (2.15)) and the height of the spherical cap is $D + \delta - \delta_v$. Thus, the turbulent lift is expressed as[31,32]

$$F_{LT} = -\left(\frac{\partial p}{\partial z}\right)_{z=z_{D2}}(D + \delta - \delta_v)\frac{\pi}{4}T^2 = \rho_f\left(\frac{\mathrm{D}w}{\mathrm{D}t}\right)_{z=z_{D2}}(D + \delta - \delta_v)\frac{\pi}{4}T^2. \tag{2.47}$$

The F_{LT} in nondimensional form is

$$F^+_{LT}\left(= \frac{F_{LT}}{\rho_f u_*^2 D^2}\right) = \frac{\pi}{4}(1 + \delta^+ - \delta^+_v)T^{+2}\left(\frac{\mathrm{D}w^+}{\mathrm{D}t^+}\right)_{z^+_0 = z^+_{D2}}. \tag{2.48}$$

Thus, the total lift force F_L in nondimensional form is

$$F^+_L\left(= \frac{F_L}{\rho_f u_*^2 D^2}\right) = F^+_{LS} + F^+_{LM} + F^+_{LC} + F^+_{LT}. \tag{2.49}$$

The point of action of the lift force is at the center of the solitary particle (see Fig. 3).[14,15,17,18,24,30] It may be noted that the order of magnitude of hydrodynamic forces in terms of scaling laws is analyzed in Appendix B.

C. Determination of threshold Shields parameter

For the sediment threshold in rolling mode, the moment balance of the force system about the pivoting point is $F_D L_z + F_L L_x = F_G L_x$, where L_x and L_z are the horizontal and the vertical lever arms, respectively (Fig. 1). Substituting Eq. (2.8) into the above condition yields

$$\Theta_c \left(= \frac{u_*^2}{\Delta g D} \right) = \frac{\pi L_x^+}{6(F_L^+ L_x^+ + F_D^+ L_z^+)}, \tag{2.50}$$

where L_x^+ is L_x/D and L_z^+ is L_z/D.

D. Determination of lever arms

The horizontal lever arm L_x of the force system is r_{IK} (see Fig. 1). Using the geometrical configuration, the L_x in nondimensional form is expressed as

$$L_x^+ = \frac{\sqrt{3}}{2\pi} \frac{k_s^+}{1 + k_s^+} \ln(2 + \sqrt{3}). \tag{2.51}$$

The vertical lever arm L_z of the force system is $r_{C'I}$ (see Fig. 1). Again using the geometrical configuration, the L_z in nondimensional form is expressed as

$$L_z^+ = z_D^+ - \delta^+ + \frac{1}{2\sqrt{3}} \frac{(3 + 6k_s^+ - k_s^{+2})^{0.5}}{1 + k_s^+} - 0.5. \tag{2.52}$$

E. Determination of mean velocity and velocity gradient

The mean velocity $\bar{u}_m$ received by the solitary particle is determined as (see Fig. 2)

$$\bar{u}_m = \frac{S_c}{A_{z=\xi k_s}} \int_{\xi k_s}^{D+\delta} \bar{u} \mathrm{d}A = \frac{2S_c}{A_{z=\xi k_s}} \int_{\xi k_s}^{D+\delta} \bar{u}[(z-\delta)(D+\delta-z)]^{0.5} \mathrm{d}z, \tag{2.53}$$

where S_c is the hindrance coefficient being less than unity.[12,31] The reason to introduce the hindrance coefficient S_c in this study is twofold. First, the presence of bed sediment particles upstream of the solitary particle results in a reduction of flow area received by the solitary particle. Second, the velocity field in the vicinity of the sediment bed is substantially affected by the surface of the bed particles. As a consequence, the mean velocity received by the solitary particle (in the yz-plane) reduces to some extent. Thus, the mean velocity obtained from the velocity law is multiplied by the hindrance coefficient to incorporate the aforementioned effects. Since a deterministic formulation of S_c is a difficult proposition, a sensitivity analysis of S_c on the threshold curve with respect to the experimental data is performed.

Thus, the $\bar{u}_m$ in nondimensional form is

$$\bar{u}_m^+ = \frac{2S_c}{A^+_{z_0^+=\xi k_s^+}} \int_{\xi k_s^+}^{1+\delta^+} \bar{u}^+[(z_0^+ - \delta^+)(1+\delta^+ - z_0^+)]^{0.5} \mathrm{d}z_0^+. \tag{2.54}$$

The velocity gradient $\partial\bar{u}/\partial z$ is then obtained as

$$\frac{\partial \bar{u}}{\partial z} = \frac{1}{D+\delta-\xi k_s} \int_{\xi k_s}^{D+\delta} \frac{\partial \bar{u}}{\partial z} \mathrm{d}z = \frac{\bar{u}_{z=D+\delta} - \bar{u}_{z=\xi k_s}}{D+\delta-\xi k_s}. \tag{2.55}$$

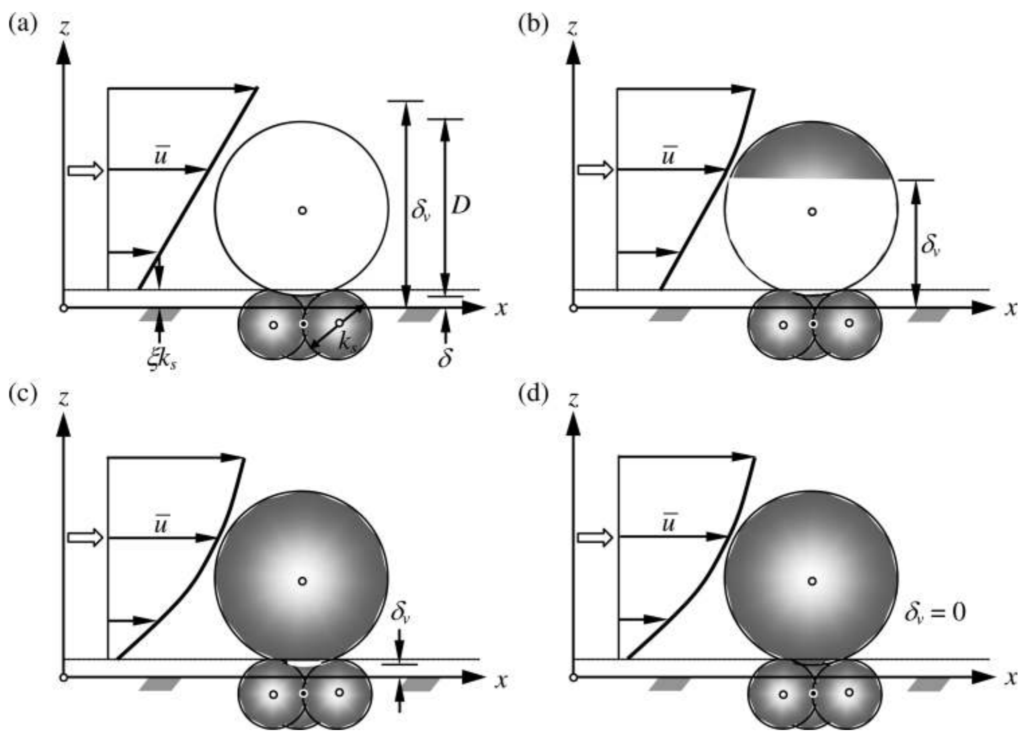

FIG. 4. Schematic of flow velocity received by the solitary particle in the xz-plane for (a) $\delta_v \geq D$, (b) $\xi k_s < \delta_v < D$, (c) $0 < \delta_v < \xi k_s$, and (d) $\delta_v = 0$.

Thus, the $\partial \bar{u}/\partial z$ in nondimensional form is

$$\frac{\partial \bar{u}^+}{\partial z_0^+} = \frac{\bar{u}^+_{z_0^+=1+\delta^+} - \bar{u}^+_{z_0^+=\xi k_s^+}}{1+\delta^+ - \xi k_s^+}. \tag{2.56}$$

Figure 4 shows the schematic of flow velocity received by the solitary particle in the xz-plane. To obtain the threshold Shields parameter Θ_c for different flow regimes (that is, hydraulically smooth, transitional, and rough flow regimes), we have the following cases:

Case 1 ($\delta_v \geq D$): In this case, the solitary particle is submerged within the viscous sublayer and the particle does not experience any velocity fluctuations (see Fig. 4(a)). It, therefore, corresponds to the hydraulically smooth flow regime, where the viscous effect is predominant in the vicinity of the bed. The velocity law for this case is expressed as[14,15]

$$\bar{u}^+ = \frac{u_* z}{\upsilon} = \frac{R_*}{k_s^+} z_0^+. \tag{2.57}$$

The mean velocity $\bar{u}_m^+$ determined from Eq. (2.54) is

$$\bar{u}_m^+ = \frac{2S_c R_*}{A^+_{z_0^+=\xi k_s^+} k_s^+} \int_{\xi k_s^+}^{1+\delta^+} z_0^+ [(z_0^+ - \delta^+)(1+\delta^+ - z_0^+)]^{0.5} \mathrm{d}z_0^+. \tag{2.58}$$

The velocity gradient $\partial \bar{u}^+/\partial z_0^+$ obtained from Eq. (2.56) is

$$\frac{\partial \bar{u}^+}{\partial z_0^+} = \frac{\bar{u}^+_{z_0^+=1+\delta^+} - \bar{u}^+_{z_0^+=\xi k_s^+}}{1+\delta^+ - \xi k_s^+} = \frac{R_*}{k_s^+}. \tag{2.59}$$

Case 2 ($0 < \delta_v < D$): In this case, the solitary particle is partially exposed to the turbulent flow. It, therefore, corresponds to the hydraulically transitional flow regime, where the effects of both the viscosity and the roughness are predominant in the vicinity of the bed. The velocity law for this case is expressed as follows:[66]

$$\bar{u}^+ = \frac{1}{\kappa\zeta_{z_0^+=z_0^+}}(0.5 - \sqrt{\zeta^2_{z_0^+=z_0^+} + 0.25}) + \frac{1}{\kappa}\ln(2\zeta_{z_0^+=z_0^+} + 2\sqrt{\zeta^2_{z_0^+=z_0^+} + 0.25}) + R_v, \quad (2.60)$$

where κ is the von Kármán constant, $\zeta = \kappa R_*(z_0^+ - \delta_v^+)/k_s^+$, and $R_v = u_*\delta_v/\upsilon$.

Moreover, this regime can be divided into two sub-regimes:

(a) For $\xi k_s < \delta_v < D$ (see Fig. 4(b)), the mean velocity $\bar{u}_m^+$ derived from Eq. (2.54) is

$$\begin{aligned}\bar{u}_m^+ = {} & \frac{2S_c R_*}{(A^+_{z_0^+=\xi k_s^+} - A^+_{z_0^+=\delta_v^+})k_s^+}\int_{\xi k_s^+}^{\delta_v^+} z_0^+[(z_0^+ - \delta^+)(1+\delta^+ - z_0^+)]^{0.5}\mathrm{d}z_0^+ \\ & + \frac{2S_c}{A^+_{z_0^+=\delta_v^+}}\int_{\delta_v^+}^{1+\delta^+}[(z_0^+ - \delta^+)(1+\delta^+ - z_0^+)]^{0.5}\left\{\frac{1}{\kappa\zeta_{z_0^+=z_0^+}}(0.5 - \sqrt{\zeta^2_{z_0^+=z_0^+} + 0.25})\right. \\ & \times \left.\frac{1}{\kappa}\ln(2\zeta_{z_0^+=z_0^+} + 2\sqrt{\zeta^2_{z_0^+=z_0^+} + 0.25}) + R_v\right\}\mathrm{d}z_0^+. \end{aligned} \quad (2.61)$$

The velocity gradient $\partial\bar{u}^+/\partial z_0^+$ determined from Eq. (2.56) is

$$\begin{aligned}\frac{\partial\bar{u}^+}{\partial z_0^+} = {} & \frac{R_*}{k_s^+} + \frac{1}{1+\delta^+ - \delta_v^+}\left\{\frac{1}{\kappa\zeta_{z_0^+=\xi k_s^+}}(0.5 - \sqrt{\zeta^2_{z_0^+=\xi k_s^+} + 0.25})\right. \\ & \left. + \frac{1}{\kappa}\ln\,(2\zeta_{z_0^+=\xi k_s^+} + 2\sqrt{\zeta^2_{z_0^+=\xi k_s^+} + 0.25})\right\}. \end{aligned} \quad (2.62)$$

(b) For $0 < \delta_v \leq \xi k_s$ (see Fig. 4(c)), the mean velocity $\bar{u}_m^+$ derived from Eq. (2.54) is

$$\begin{aligned}\bar{u}_m^+ = {} & \frac{2S_c}{A^+_{z_0^+=\xi k_s^+}}\int_{\xi k_s^+}^{1+\delta^+}[(z_0^+ - \delta^+)(1+\delta^+ - z_0^+)]^{0.5}\left\{\frac{1}{\kappa\zeta_{z_0^+=z_0^+}}(0.5 - \sqrt{\zeta^2_{z_0^+=z_0^+} + 0.25})\right. \\ & \left. + \frac{1}{\kappa}\ln\,(2\zeta_{z_0^+=z_0^+} + 2\sqrt{\zeta^2_{z_0^+=z_0^+} + 0.25}) + R_v\right\}\mathrm{d}z_0^+. \end{aligned} \quad (2.63)$$

The velocity gradient $\partial\bar{u}^+/\partial z_0^+$ obtained from Eq. (2.56) is

$$\frac{\partial\bar{u}^+}{\partial z_0^+} = \frac{1}{1+\delta^+ - \xi k_s^+}\left\{\frac{1}{\kappa\zeta_{z_0^+=\xi k_s^+}}(0.5 - \sqrt{\zeta^2_{z_0^+=\xi k_s^+} + 0.25}) + \frac{1}{\kappa}\ln(2\zeta_{z_0^+=\xi k_s^+} + 2\sqrt{\zeta^2_{z_0^+=\xi k_s^+} + 0.25})\right\}. \quad (2.64)$$

The experimental observation of Nikuradse[67] on pipe flow showed that the R_v decreases monotonically with R_*. The experimental data $R_v(R_*)$ of Nikuradse[67] are shown in Fig. 5. The American Society of Civil Engineers (ASCE) Task Force[68] on friction factor in open channels reported that for open-channel roughness similar to that encountered in pipes, the resistance equations similar to those of pipe flows are adequate. Figure 5 shows that the experimental data have an agreement with a quartic polynomial which has the following form:

$$R_v = a_0 + a_1R_* + a_2R_*^2 + a_3R_*^3 + a_4R_*^4\ \forall\ R_* \in (0, 54.3), \quad (2.65)$$

$$R_v = 0\ \forall\ R_* \in [54.3, \infty), \quad (2.66)$$

where $a_0 = 7.084$, $a_1 = -14.95\times10^{-2}$, $a_2 = -4.46\times10^{-3}$, $a_3 = 1.72\times10^{-4}$, and $a_4 = -1.54\times10^{-6}$.

Case 3 ($\delta_v = 0$): In this case, the solitary particle is fully exposed to the turbulent flow and the viscous sublayer does not exist (see Fig. 4(d)). It, therefore, corresponds to the hydraulically rough flow regime, where the effect of roughness is predominant in the vicinity of the bed. The velocity law

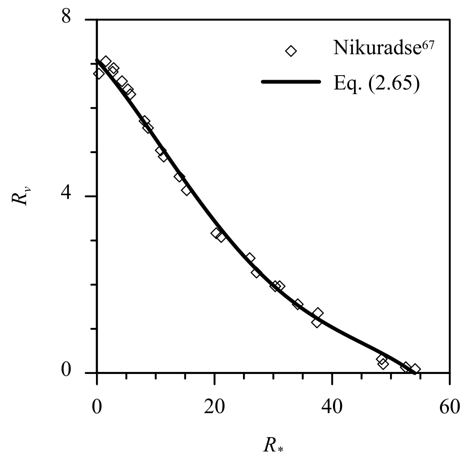

FIG. 5. Experimental data $R_\upsilon(R_*)$ of Nikuradse[67] and the fitted polynomial.

for this case is expressed as follows:[66]

$$\bar{u}^+ = \frac{1}{\kappa \eta_{z_0^+=z_0^+}}\left(0.5 - \sqrt{\eta^2_{z_0^+=z_0^+} + 0.25}\right) - \frac{1}{\kappa R_l}\left(0.5 - \sqrt{R_l^2 + 0.25}\right) + \frac{1}{\kappa}\ln\left(\frac{\eta_{z_0^+=z_0^+} + \sqrt{\eta^2_{z_0^+=z_0^+} + 0.25}}{R_l + \sqrt{R_l^2 + 0.25}}\right), \tag{2.67}$$

where η is $(R_l + \kappa R_* z_0^+)/k_s^+$, R_l is $u_* l/\upsilon$, and l is the intercept of the mixing length at $z = 0$.

The mean velocity $\bar{u}_m^+$ determined from Eq. (2.54) is

$$\bar{u}_m^+ = \frac{2S_c}{A^+_{z_0^+=\xi k_s^+}} \int_{\xi k_s^+}^{1+\delta^+} [(z_0^+ - \delta^+)(1 + \delta^+ - z_0^+)]^{0.5} \left\{ \frac{1}{\kappa \eta_{z_0^+=z_0^+}}\left(0.5 - \sqrt{\eta^2_{z_0^+=z_0^+} + 0.25}\right) - \frac{1}{\kappa R_l}\left(0.5 - \sqrt{R_l^2 + 0.25}\right) + \frac{1}{\kappa}\ln\left(\frac{\eta_{z_0^+=z_0^+} + \sqrt{\eta^2_{z_0^+=z_0^+} + 0.25}}{R_l + \sqrt{R_l^2 + 0.25}}\right) \right\} dz_0^+. \tag{2.68}$$

The velocity gradient $\partial \bar{u}^+/\partial z_0^+$ obtained from Eq. (2.56) is

$$\frac{\partial \bar{u}^+}{\partial z_0^+} = \frac{1}{1 + \delta^+ - \xi k_s^+} \left\{ \frac{1}{\kappa \eta_{z_0^+=1+\delta^+}}\left(0.5 - \sqrt{\eta^2_{z_0^+=1+\delta^+} + 0.25}\right) - \frac{1}{\kappa \eta_{z_0^+=\xi k_s^+}}\left(0.5 - \sqrt{\eta^2_{z_0^+=\xi k_s^+} + 0.25}\right) + \frac{1}{\kappa}\ln\left(\frac{\eta_{z_0^+=1+\delta^+} + \sqrt{\eta^2_{z_0^+=1+\delta^+} + 0.25}}{\eta_{z_0^+=\xi k_s^+} + \sqrt{\eta^2_{z_0^+=\xi k_s^+} + 0.25}}\right) \right\}. \tag{2.69}$$

Using the experimental data of Nikuradse,[67] Rotta[66] proposed that the R_l can be expressed in the following form:

$$R_l = 0.014R_* - 0.76 \; \forall \; R_* \in [54.3, \infty), \tag{2.70}$$

$$R_l = 0 \; \forall \; R_* \in (0, 54.3). \tag{2.71}$$

For a sediment bed at near-threshold condition, the velocity laws are modified due to the expansion of the roughness layer, resulting in a slight deviation of von Kármán constant κ value from its universal value $\kappa = 0.41$. The experimental investigations of Best *et al.*[69] and Dey *et al.*[70,71] revealed that the value of κ reduces in flows over weakly mobile beds. Best *et al.*[69] reported an average value of $\kappa = 0.385$ which is adopted in the present study. Further, van Rijn[65] stated that the virtual bed level can be fixed at a distance $0.25k_s$ below the summit of the bed particles (that is, $\xi = 0.25$) in order to preserve the velocity law over an immobile bed. However, the experimental observation of Dey *et al.*[71] revealed an upward shift of the virtual bed level for a weakly mobile bed. Here, we consider $\xi = 0.21$ as reported by Dey *et al.*[71]

III. COMPUTATIONAL STEPS

The pivoting angle ϕ_m has a wide variation depending on the variable pocket geometry and the nonuniformity of sediments. However, for uniform sediments, k_s^+ is approximately unity. To determine the threshold Shields parameter Θ_c, the computational steps are described as follows:

(1) For a given ϕ_m, determine k_s^+ from Eq. (2.7) or *vice versa*.
(2) Compute δ^+ from Eq. (2.2).
(3) For a given R_*, determine R_v from Eq. (2.65) or (2.66).
(4) Determine $\delta_v^+ = R_v k_s^+/R_*$ and find the flow regime: for smooth flow, $\delta_v^+ \geq 1$, for transitional flow, $0 < \delta_v^+ < 1$, and for rough flow, $\delta_v^+ = 0$.
(5) Compute $z_{D1}^+ (= z_{D1}/D)$ numerically from Eq. (2.12) using the expression for $\bar{u}^+$ from Eq. (2.57) for smooth flow or Eq. (2.60) for transitional flow or Eq. (2.67) for rough flow, and then determine $z_{D2}^+ (= z_{D2}/D)$ from Eq. (2.16) or (2.17).
(6) Estimate $\bar{u}_m^+$ from Eq. (2.58) for smooth flow, (2.61) or (2.63) for transitional flow, and (2.68) for rough flow.
(7) Estimate $\partial \bar{u}^+/\partial z_0^+$ from Eq. (2.59) for smooth flow, (2.62) or (2.64) for transitional flow, and (2.69) for rough flow.
(8) Evaluate C_D from Eq. (2.22).
(9) Compute C_L from $C_L = 0.85C_D$.
(10) Determine $\sigma_u^+|_{z_0^+=z_{D2}^+}$ and $\sigma_w^+|_{z_0^+=z_{D2}^+}$ from Eqs. (2.35) and (2.36), respectively.
(11) Calculate $\lambda^+_{z_0^+=z_{D2}^+}$ from Eq. (2.39) with $\lambda_0^+ = R_l/R_*$.
(12) Obtain $\overline{\mathrm{D}u^+/\mathrm{D}t^+}$ and $\overline{\mathrm{D}w^+/\mathrm{D}t^+}$ from Eqs. (2.33) and (2.34), respectively.
(13) Compute F_D^+ from Eq. (2.21).
(14) Compute F_L^+ from Eq. (2.49). Note that for Case 1 ($\delta_v \geq D$), $F_L^+ = F_{LS}^+ + F_{LM}^+ + F_{LC}^+$ since $F_{LT}^+ = 0$; and for Case 2 ($0 < \delta_v < D$) and Case 3 ($\delta_v = 0$), $F_L^+ = F_{LS}^+ + F_{LM}^+ + F_{LC}^+ + F_{LT}^+$. Further, for Case 1, $A_{z=\delta_v}$ vanishes, while for Cases 2 and 3, it exists.
(15) Calculate L_x^+ and L_z^+ from Eqs. (2.51) and (2.52), respectively.
(16) Determine Θ_c from Eq. (2.50).

IV. RESULTS AND DISCUSSION

To show the graphical representations of $\Theta_c(R_*)$, we consider the characteristic values of sediment mass density ρ_s, fluid mass density ρ_f, and kinematic viscosity υ as 2650 kg m^{-3}, 10^3 kg m^{-3} (water), and 10^{-6} m^2 s^{-1}, respectively.

Figure 6 shows the curve of threshold Shields parameter Θ_c as a function of threshold shear Reynolds number R_{*c} obtained from the present study for $S_c = 0.2, 0.3$, and 0.4 and the experimental data of uniform sediments. The experimental data are obtained from the work of Gilbert,[1] Shields,[5] Mantz,[6] Yalin and Karahan,[8] White,[20] Zanke,[25] Iwagaki,[31] Casey,[72] Kramer,[73] USWES,[74] Vanoni,[75] Meyer-Peter and Müller,[76] Neill,[77] Grass,[78] White,[79] Karahan,[80] Julien,[81] and Soulsby and Whitehouse.[82] Moreover, the explicit version of the Shields curve proposed by Hager and Del Giudice[83] (also see Hager and Oliveto[84]) is also shown for the comparison. It is evident that the $\Theta_c(R_{*c})$-curves shift downward with an increase in S_c. The $\Theta_c(R_{*c})$-curve for $S_c = 0.3$ provides an excellent fitting (as if it were a regression fitting) with the thick band of experimental data over a wide range of R_{*c}. On the other hand, the experimental data are approximately bounded by the $\Theta_c(R_{*c})$-curves for $S_c = 0.2$ and 0.4. Figure 6 shows that for $S_c = 0.3$, the Θ_c decreases with an increase in R_{*c} becoming a minimum as $\Theta_c = 0.025$ at $R_{*c} = 16$ and then gradually increases to attain a constant value as $\Theta_c = 0.044$ for $R_{*c} \geq 100$. According to the $\Theta_c(R_{*c})$-curve of Yalin and Karahan,[8] the threshold

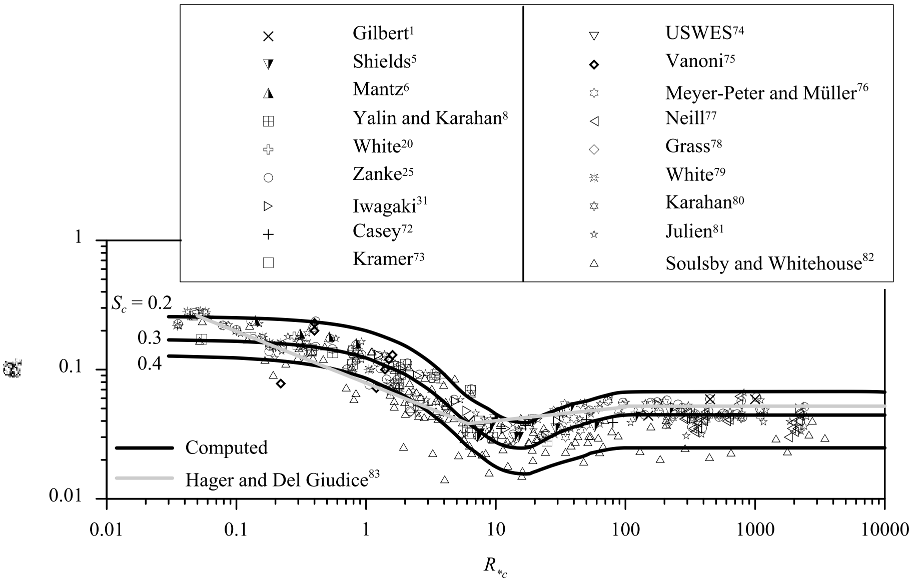

FIG. 6. Comparison of the curves of threshold Shields parameter Θ_c versus threshold shear Reynolds number R_{*c} obtained from the present study for $S_c = 0.2$, 0.3, and 0.4 with the experimental data of uniform sediments and $\Theta_c(R_{*c})$-curve of Hager and Del Giudice.[83]

Shields parameter Θ_c for hydraulically rough flow regime is independent of R_{*c} having a constant value of $\Theta_c = 0.046$, which closely corresponds to the value of $\Theta_c = 0.044$ obtained from this study. Further, the $\Theta_c(R_{*c})$-curve given by Hager and Del Giudice,[83] in general, underestimates the experimental data in hydraulically smooth flow regime but slightly overestimates in hydraulically transitional and rough flow regimes. It may be noted that the simulated natural bed conditions in the experiments corresponding to the data plots in Fig. 6 might not be under the same idealized condition as considered in Fig. 4 of this study. As such, the experimental data scatter in Fig. 6 reveals that a universal threshold curve for the determination of threshold Shields parameter is a difficult proposition. Therefore, it is desirable to obtain the upper and lower bounds of the threshold curve. For

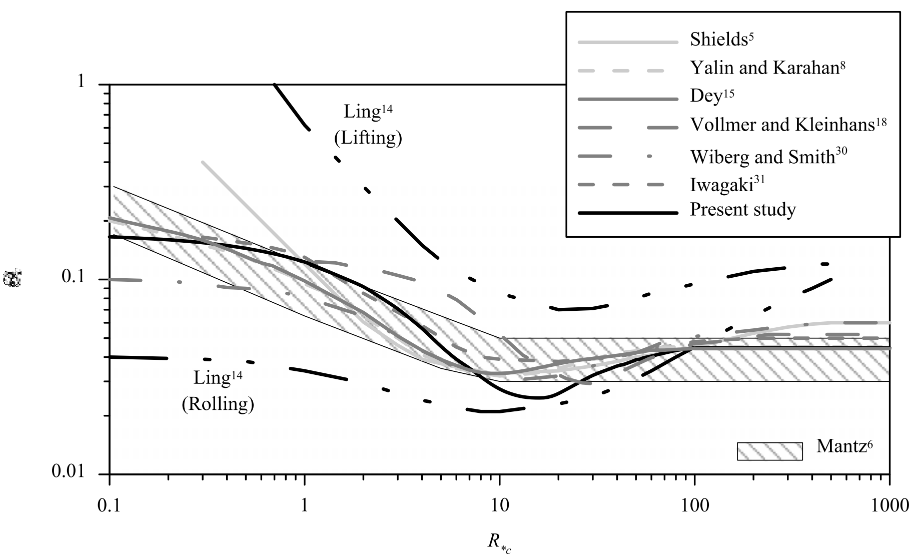

FIG. 7. Comparison of the curve of threshold Shields parameter Θ_c versus threshold shear Reynolds number R_{*c} for $S_c =$ 0.3 obtained from the present study with those of various researchers.

instance, Mantz[6] proposed the *extended Shields diagram* (see the shaded band in Fig. 7) to obtain the condition of maximum stability of sediment particles. Using the extensive experimental data of gravel-bed rivers, Buffington and Montgomery[10] reported that for the rough flow regime, the reference based and visual based studies have typical ranges of threshold Shields parameter as 0.052–0.086 and 0.03–0.073, respectively. Furthermore, Dey and Raikar[85] showed that in the rough flow regime, most of the experimental data at near-threshold condition are confined within the curves of Shields[5] and Yalin and Karahan.[8] Therefore, Dey and Raikar[85] used the lower, intermediate, and upper threshold conditions to distinguish the experimental data. Reverting back to this study, Fig. 6 shows that the experimental data are approximately confined within the two threshold curves, corresponding to $S_c = 0.4$ (upper bound) and 0.2 (lower bound). The values of threshold Shields parameter for the rough flow regime, obtained from this study, corresponding to $S_c = 0.4$ and 0.2 are 0.025 and 0.067, respectively. Therefore, it can be concluded that the S_c can be varied to simulate range of experimental condition.

Figure 7 presents the comparison of the curve of threshold Shields parameter Θ_c versus threshold shear Reynolds number R_{*c} obtained from this study with those of various researchers.[5,6,8,14,15,18,30,31] To prepare Fig. 7, we consider $S_c = 0.3$. Figure 7 shows that the $\Theta_c(R_{*c})$-curve obtained from this study lies within the shaded zone, referred to the *extended Shields diagram*,[6] excepting $8 < R_{*c} < 25$. The $\Theta_c(R_{*c})$-curve proposed by Dey[15] falls within the shaded zone of Mantz,[6] since an extensive calibration of the lift coefficient with the experimental data was done by Dey.[15] The $\Theta_c(R_{*c})$-curve of Ling[14] shows two limits, such as rolling and lifting. Ling[14] argued that the real feature of sediment threshold lies within the curves defining the rolling and lifting threshold. However, it is difficult to find the value of Θ_c from the $\Theta_c(R_{*c})$-curves of Ling[14] because the actual threshold curve is hidden within the rolling and lifting threshold curves. It is pertinent to state that both the rolling and lifting threshold curves of Ling[14] monotonically increase with an increase in R_{*c} in the hydraulically rough flow regime. This phenomenon is not practically feasible, as the Θ_c in the hydraulically rough flow regime is independent of R_{*c}. Furthermore, the $\Theta_c(R_{*c})$-curve of Wiberg and Smith[30] and Vollmer and Kleinhans[18] predicts a monotonic increase in Θ_c with R_{*c} for $R_{*c} \geq 100$. However, Vollmer and Kleinhans[18] reported that the dip in the $\Theta_c(R_{*c})$-curve occurs at higher R_{*c} than that predicted by the Shields diagram.[5] This study is in conformity with this fact, as Fig. 7 shows that the dip in the $\Theta_c(R_{*c})$-curve of Shields[5] occurs early than that of this study.

Figure 8 illustrates the curves of threshold Shields parameter Θ_c versus threshold shear Reynolds number R_{*c} for $k_s^+ = 0.25$, 0.5, 1, and 2 (or mean pivoting angles $\phi_m = 8.6$, 15.25, 26, and 38.7° as obtained from Eq. (2.7)) and $S_c = 0.3$ obtained from the present study. It is evident that the Θ_c increases with an increase in k_s^+. This is due to the fact that an increase in k_s^+ indicates that the size of

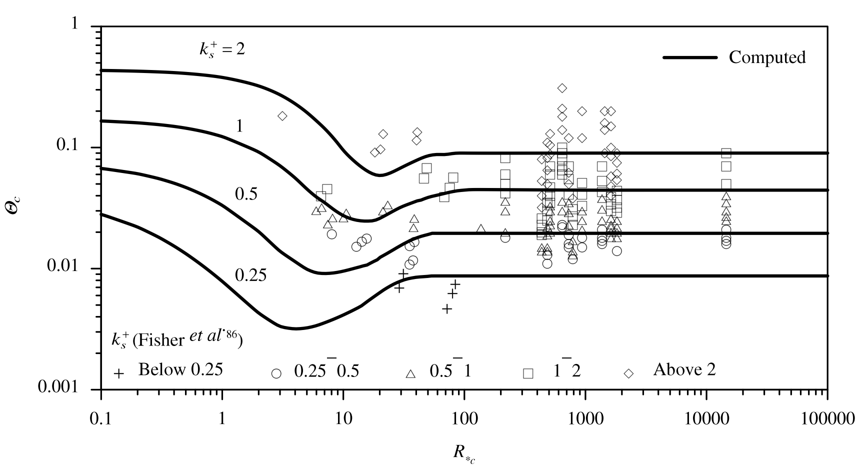

FIG. 8. Comparison of the curves of threshold Shields parameter Θ_c versus threshold shear Reynolds number R_{*c} for $k_s^+ = 0.25$, 0.5, 1, and 2 and $S_c = 0.3$ obtained from the present study with the experimental data of Fisher *et al.*[86] for nonuniform sediments grouped into different k_s^+ classes.

the solitary particle is much smaller than that of the bed particles. As a consequence, with an increase in k_s^+, the solitary particle becomes more hidden within the bed pocket geometry. Thus, a greater bed shear stress is required to dislodge the particle. The threshold Shields parameter Θ_c in the rough flow regime for $k_s^+ = 0.25, 0.5, 1$, and 2, obtained from this study is 0.009, 0.019, 0.044, and 0.089, respectively. Another important observation is that the occurrence of dip in $\Theta_c(R_{*c})$-curve is delayed with an increase in k_s^+. The experimental data of $\Theta_c(R_{*c})$ for nonuniform sediments reported by Fisher *et al.*[86] are grouped into different k_s^+ classes. The comparison of the computed $\Theta_c(R_{*c})$-curves obtained from this study with the experimental data shows that the computed $\Theta_c(R_{*c})$-curves, in general, do a good job in separating the experimental data of different k_s^+ classes of nonuniform sediments.

The novelty of this study as compared to the previous studies lies on the fact that this study analyses the threshold motion of sediment particles in 3D configuration by applying the fundamental concepts of hydrodynamics and micro-mechanics. The hydrodynamic force is resolved into drag (collective effects of form drag and form induced drag) and lift (collective effects of Saffman lift, Magnus lift, centrifugal lift, and turbulent lift) taking part to the micro-mechanical force system that governs the initiation of sediment particle motion. It thus provides a clear physical insight into the sediment threshold phenomenon. The evolution of different force components depending on the shear Reynolds number is well focused. The consideration of viscous sublayer and its decay with the shear Reynolds number in an explicit form is incorporated into the mathematical analysis. The points of action of the hydrodynamic forces being the key feature are obtained from the basics of mechanics, for the first time to the best of authors' knowledge. The consideration of velocity fluctuations (turbulence) from the concept of statistical theory of turbulence makes the formulation more realistic. Further, the reduction in mean velocity received by the solitary particle due to the bed particles and resistance to flow is incorporated by introducing the hindrance coefficient. Given above, this study provides therefore an improved treatment of the sediment threshold problem over the existing ones.

It is pertinent to mention that the present mathematical model is applicable for a steady turbulent flow over a closely packed plane sediment bed formed by uniform and nonuniform sediment particles. However, an exact determination of hindrance coefficient used in this study requires more experimental evidences. The model results are thus limited to the closely packed sediment beds. However, for nonuniform sediment particles subjected to different bed packing conditions forming a loosely packed sediment bed, the present mathematical model can be further extended, as a future scope of research study.

V. CONCLUSIONS

A novel mathematical model is presented to determine the threshold bed shear stress to initiate cohesionless sediment particle motion under a steady unidirectional streamflow over a sediment bed. The sediment particles are considered as discrete spherical particles. The primary mode of sediment threshold is considered as rolling mode. The forces acting on a solitary sediment particle resting over three identical closely packed bed particles are analyzed from the basics of the hydrodynamics and micro-mechanics. The form drag and form induced drag contribute to the hydrodynamic drag force. On the other hand, the hydrodynamic lift force comprises of Saffman lift, Magnus lift, centrifugal lift, and turbulent lift. The effects of velocity fluctuations are incorporated in the analysis by applying the statistical theory of turbulence. The governing equation of sediment threshold is obtained by taking moment of the force system on the solitary particle about the pivoting point. To investigate the sediment threshold under hydraulically smooth, transitional, and rough flow regimes, three different velocity laws are used in the analysis. The $\Theta_c(R_{*c})$-curve obtained from the present study compares well with those of previous studies. The present model provides a satisfactory agreement with the experimental data of uniform and nonuniform sediments.

APPENDIX A: LIMITATIONS OF THE PREVIOUS STUDIES

The limitations of the previous studies on modeling the sediment threshold are listed in Table I. The mathematical model presented in this study overcomes these limitations.

TABLE I. Limitations of the previous studies on modeling the sediment threshold.

References	Limitations
Ling[14]	Considered 2D configuration of sediment bed and disregarded form induced drag, turbulent lift, appropriate points of action of force system, determination of mean velocity from area-averaged concept, decay of viscous sublayer with shear Reynolds number, velocity fluctuations (turbulence effects), and hindrance coefficient
Dey[15]	Ignored form induced drag, centrifugal lift, turbulent lift, appropriate points of action of force system, decay of viscous sublayer with shear Reynolds number and velocity fluctuations (turbulence effects)
Wu and Chou[17]	Considered 2D configuration of sediment bed, a single velocity law for the hydraulically rough flow regime and constant streamwise turbulence intensity in the vicinity of the bed; and ignored vertical velocity fluctuations, appropriate points of action of force system, form induced drag, Magnus lift, centrifugal lift, turbulent lift, decay of viscous sublayer with shear Reynolds number, and hindrance coefficient
Vollmer and Kleinhans[18]	Considered 2D moment arms and pivoting angle, a single velocity law for the hydraulically rough flow regime and constant turbulence intensity in the vicinity of the bed; and disregarded appropriate points of action of force system, form induced drag, Magnus lift, centrifugal lift, decay of viscous sublayer with shear Reynolds number, and hindrance coefficient
White[20]	Considered 2D configuration of sediment bed and ignored form induced drag, Magnus lift, centrifugal lift, turbulent lift, appropriate points of action of force system, and decay of viscous sublayer with shear Reynolds number
Zanke[25]	Considered 2D configuration of sediment bed and disregarded form induced drag, Magnus lift, centrifugal lift, turbulent lift, appropriate points of action of force system, determination of mean velocity from area-averaged concept, and decay of viscous sublayer with shear Reynolds number
Wiberg and Smith[30]	Considered 2D configuration of sediment bed and disregarded form induced drag, Magnus lift, centrifugal lift, turbulent lift, appropriate points of action of force system, decay of viscous sublayer with shear Reynolds number, and velocity fluctuations (turbulence effects)
Iwagaki[31]	Considered 2D configuration of sediment bed and ignored lift force in hydraulically smooth flow regime, Saffman lift, Magnus lift, centrifugal lift, appropriate points of action of force system, and determination of mean velocity from area-averaged concept
Luckner[37]	Improperly determined the points of action of force system and disregarded form induced drag, Magnus lift, centrifugal lift, turbulent lift, and decay of viscous sublayer with shear Reynolds number

APPENDIX B: ORDER OF MAGNITUDE OF HYDRODYNAMIC FORCES

The time-averaged velocity $\bar{u}$, the mean velocity $\bar{u}_m$, and the velocity of fluid V at the center of the particle can be written as $(\bar{u}, \bar{u}_m, V) \sim u_*$, where the symbol "$\sim$" represents the "scales with". Since $\lambda_0^+ = R_l/R_*$ (see computational step 11), we can write $\lambda_0^+ \sim R_*^{-1}$, using Eq. (2.70). Therefore, from Eq. (2.39), we obtain $\lambda^+ \sim \lambda_0^+$. Considering $k_s = D$ ($k_s^+ = 1$) for simplicity, the turbulence intensity components (σ_u, σ_w) can be scaled as $(\sigma_u, \sigma_w) \sim u_*$. Thus, Eqs. (2.33) and (2.34) reduce to $\overline{Du^+/Dt^+} \sim R_*$ and $\overline{Dw^+/Dt^+} \sim R_*$. Using the above scaling laws, the form drag F_{D1} in nondimensional form can be written as $F_{D1}^+ \sim C_D$, where F_{D1}^+ is $F_{D1}/\rho_f u_*^2 D^2$. Since C_D is a function of R_* (see Eq. (2.22)), the F_{D1}^+ reduces with R_* becoming a constant in the hydraulically rough flow regime. The form induced drag F_{D2} in nondimensional form is $F_{D2}^+ \sim R_*$, where F_{D2}^+ is $F_{D2}/\rho_f u_*^2 D^2$. Since the F_{D2}^+ is practically zero for the hydraulically smooth flow, the above scaling of F_{D2}^+ indicates that the F_{D2}^+ increases with R_* in the hydraulically transitional flow regime. However, it attains almost a constant value in the hydraulically rough flow regime. Furthermore, the velocity gradient can be scaled with the bed shear stress, that is $\partial\bar{u}/\partial z \sim u_*^2/\upsilon$. Thus, $\partial\bar{u}^+/\partial z_0^+ \sim R_*$. Hence, from Eqs. (2.41), (2.43), (2.46), and (2.48), we obtain $F_{LS}^+ \sim C_L$, $F_{LM}^+ \sim R_*$, $F_{LC}^+ \sim R_*^2$, and $F_{LT}^+ \sim R_*$. Since $C_L \sim C_D$, the F^+_{LS} reduces with R_* in the hydraulically transitional flow regime, whereas the F^+_{LM}, F^+_{LC}, and F^+_{LT} increase with R_*. However, they attain almost a constant value in the hydraulically rough flow regime.

NOMENCLATURE

A_z	=	projected area of solitary particle bounded within $z = D + \delta$ and any vertical distance z
A^+	=	A/D^2
C_D	=	drag coefficient
C_L	=	lift coefficient
D	=	solitary particle diameter
F_D	=	drag force
F^+_D	=	$F_D/\rho_f u_*^2 D^2$
F_{D1}	=	form drag
F^+_{D1}	=	$F_{D1}/\rho_f u_*^2 D^2$
F_{D2}	=	form induced drag
F^+_{D2}	=	$F_{D2}/\rho_f u_*^2 D^2$
F_G	=	submerged weight of sediment particles
F_L	=	lift force
F^+_L	=	$F_L/\rho_f u_*^2 D^2$
F_{LC}	=	centrifugal lift
F^+_{LC}	=	$F_{LC}/\rho_f u_*^2 D^2$
F_{LM}	=	Magnus lift
F^+_{LM}	=	$F_{LM}/\rho_f u_*^2 D^2$
F_{LS}	=	Saffman lift
F^+_{LS}	=	$F_{LS}/\rho_f u_*^2 D^2$
F_{LT}	=	turbulent lift
F^+_{LT}	=	$F_{LT}/\rho_f u_*^2 D^2$
g	=	gravitational acceleration
h	=	flow depth
k_s	=	bed particle diameter
k^+_s	=	k_s/D
L_x	=	horizontal lever arm
L^+_x	=	L_x/D
L_z	=	vertical lever arm
L^+_z	=	L_z/D
l	=	intercept of mixing length at $z = 0$
$\bar{p}$	=	time-averaged pressure intensity
$\mathfrak{R}$	=	radius of curvature of locus of moving solitary particle over bed particles
R_*	=	shear Reynolds number (= $u_* k_s/\upsilon$)
R_l	=	$u_* l/\upsilon$
R_υ	=	$u_* \delta_\upsilon/\upsilon$
r_{AB}	=	distance between points A and B
S_c	=	hindrance coefficient
T	=	width of elementary strip across solitary particle at $z = \delta_\upsilon$
T^+	=	T/D
t^+	=	$t u_*/D$
$\bar{u}^+$	=	$\bar{u}/u_*$
$\bar{u}^+_m$	=	$\bar{u}_m/u_*$
u_*	=	shear velocity
$\bar{u}_m$	=	mean velocity received by solitary particle
u, w	=	instantaneous velocity components in (x, z)
$\bar{u}, \bar{w}$	=	time-averaged velocity components in (x, z)
u', w'	=	velocity fluctuations in (x, z)

u^+, w^+ = $(u, w)/u_*$
V = velocity of fluid at center of solitary particle
V^+ = V/u_*
x, y, z = Cartesian coordinates
z^+ = z/k_s
z_0^+ = z/D
z_D = point of action of drag force
z_{D1} = point of action of form drag
z_{D2} = point of action of form induced drag
Δ = submerged relative density of sediment particles $[= (\rho_s - \rho_f)/\rho_f]$
Θ_c = threshold Shields parameter
Ω_m = mean angular velocity of solitary particle
α_m = added mass coefficient
δ = distance of bottommost point of solitary particle from virtual bed level
δ^+ = δ/D
δ_v^+ = δ_v/D
δ_v = viscous sublayer thickness
ε = turbulent kinetic energy dissipation rate
ϕ = pivoting angle
ϕ_m = mean pivoting angle
ϕ_{max} = maximum value of pivoting angle
ϕ_{min} = minimum value of pivoting angle
η = $(R_l + \kappa R_* z_0^+)/k_s^+$
κ = von Kármán constant
λ = Taylor micro-scale
λ^+ = λ/k_s
λ_0 = amount of increase in size of eddies depending on bed roughness
λ_0^+ = λ_0/k_s
ρ_f = mass density of fluid
ρ_s = mass density of sediment particles
σ_u, σ_w = turbulence intensity components in (x, z)
σ_u^+, σ_w^+ = $(\sigma_u, \sigma_w)/u_*$
υ = kinematic viscosity of fluid
ϖ = relative submergence $(= h/k_s)$
ζ = $\kappa R_* (z_0^+ - \delta_v^+)/k_s^+$

[1] G. K. Gilbert, "The transportation of debris by running water," in *Professional paper number 86* (United States Geological Survey, Washington DC, USA, 1914).
[2] A. Schoklitsch, *Über Schleppkraft Und Geschiebebewegung* (Engelmann, Leipzig, Germany, 1914).
[3] F. Schaffernak, *Neue Grundlagen für die Berechnung der Geschiebeführung in Flussläufen* (Deutike, Vienna, Austria, 1922).
[4] H. Krey, "Grenzen der Übertragbarkeit der Versuchsergebnisse und Modellähnlichkeit bei praktischen Flussbauversuchen," Z. Angew. Math. Mech **5**, 484–486 (1925).
[5] A. F. Shields, "Application of similarity principles and turbulence research to bed-load movement," in *Mitteilungen der Preussischen Versuchsanstalt für Wasserbau und Schiffbau* (Germany, Berlin, 1936), Vol. 26, pp. 5–24.
[6] P. A. Mantz, "Incipient transport of fine grains and flakes by fluids-extended Shields diagram," J. Hydraul. Div., Am. Soc. Civ. Eng. **103**, 601–615 (1977).
[7] M. C. Miller, I. N. Mccave, and P. D. Komar, "Threshold of sediment motion under unidirectional currents," Sedimentology **24**, 507–527 (1977).
[8] M. S. Yalin and E. Karahan, "Inception of sediment transport," J. Hydraul. Div., Am. Soc. Civ. Eng. **105**, 1433–1443 (1979).
[9] W. H. Graf, *Hydraulics of Sediment Transport* (McGraw-Hill Book Company, New York, USA, 1971).
[10] J. M. Buffington and D. R. Montgomery, "A systematic analysis of eight decades of incipient motion studies, with special reference to gravel-bedded rivers," Water Resour. Res. **33**, 1993–2029, doi:10.1029/96WR03190 (1997).
[11] M. H. Garcia, *Sedimentation Engineering: Processes, Measurements, Modeling, and Practice* (ASCE Manual of Practice 110, Reston, USA, 2008).
[12] S. Dey, *Fluvial Hydrodynamics: Hydrodynamic and Sediment Transport Phenomena* (Springer-Verlag, Berlin, Germany, 2014).
[13] N. L. Coleman, "A theoretical and experimental study of drag and lift forces acting on a sphere resting on a hypothetical stream bed," in *Proceedings of the 12th Congress of International Association for Hydraulic Research* (Fort Collins, Colorado, 1967), Vol. 3, pp. 185–192.

[14] C. H. Ling, "Criteria for incipient motion of spherical sediment particles," J. Hydraul. Eng. **121**, 472–478 (1995).
[15] S. Dey, "Sediment threshold," Appl. Math. Model. **23**, 399–417 (1999).
[16] C. Ancey, F. Bigillon, P. Frey, J. Lanier, and R. Ducret, "Saltating motion of a bead in a rapid water stream," Phys. Rev. E **66**, 036306 (2002).
[17] F. C. Wu and Y. J. Chou, "Rolling and lifting probabilities for sediment entrainment," J. Hydraul. Eng. **133**, 329–334 (2003).
[18] S. Vollmer and M. G. Kleinhans, "Predicting incipient motion, including the effect of turbulent pressure fluctuations in the bed," Water Resour. Res. **43**, W05410, doi:10.1029/2006WR004919 (2007).
[19] H. Lee and S. Balachandar, "Critical shear stress for incipient of a particle on a rough bed," J. Geophys. Res. **117**, F01026, doi:10.1029/2011JF002208 (2012).
[20] C. M. White, "The equilibrium of grains on the bed of a stream," Proc. R. Soc. London, Ser. A **174**, 322–338 (1940).
[21] R. G. Jackson, "Sedimentological and fluid-dynamic implications of turbulent bursting phenomenon in geophysical flows," J. Fluid Mech. **77**, 531–560 (1976).
[22] N. S. Cheng and Y. M. Chiew, "Pickup probability for sediment entrainment," J. Hydraul. Eng. **124**, 232–235 (1998).
[23] P. Sechet and B. le Guennec, "Bursting phenomenon and incipient motion of solid particles in bed-load transport," J. Hydraul. Res. **37**, 683–696 (1999).
[24] A. N. Papanicolaou, P. Diplas, N. Evaggelopoulos, and S. Fotopoulos, "Stochastic incipient motion criterion for spheres under various bed packing conditions," J. Hydraul. Eng. **128**, 369–380 (2002).
[25] U. C. E. Zanke, "On the influence of turbulence on the initiation of sediment motion," Int. J. Sed. Res. **18**, 17–31 (2003).
[26] F. C. Wu and K. H. Yang, "Entrainment probabilities of mixed-size sediment incorporating near-bed coherent flow structures," J. Hydraul. Eng. **130**, 1187–1197 (2004).
[27] M. W. Schmeeckle, J. M. Nelson, and R. L. Shreve, "Forces on stationary particles in near-bed turbulent flows," J. Geophys. Res. **112**, F02003, doi:10.1029/2006JF000536 (2007).
[28] F. C. Wu and M. R. Jiang, "Numerical investigation of the role of turbulent bursting in sediment entrainment," J. Hydraul. Eng. **129**, 110–119 (2007).
[29] H. Jeffreys, "On the transport of sediments by streams," Proc. Cambridge Philos. Soc. **25**, 272–276 (1929).
[30] P. L. Wiberg and J. D. Smith, "Calculations of the critical shear stress for motion of uniform and heterogeneous sediments," Water Resour. Res. **23**, 1471–1480, doi:10.1029/WR023i008p01471 (1987).
[31] Y. Iwagaki, "Fundamental study on critical tractive force," Trans. Jpn. Soc. Civ. Eng. **41**, 1–21 (1956).
[32] S. Ikeda, "Incipient motion of sand particles on side slopes," J. Hydraul. Div., Am. Soc. Civ. Eng. **108**, 95–114 (1982).
[33] J. D. Fenton and J. E. Abbott, "Initial movement of grains on a stream bed: The effect of relative protrusion," Proc. R. Soc. London, Ser. A **352**, 523–537 (1977).
[34] J. W. Kirchner, W. E. Dietrich, F. Iseya, and H. Ikeda, "The variability of critical shear stress, friction angle, and grain protrusion in water-worked sediments," Sedimentology **37**, 647–672 (1990).
[35] P. D. Komar and P. A. Carling, "Grain sorting in gravel-bed streams and the choice of particle sizes for flow-competence evaluations," Sedimentology **38**, 489–502 (1991).
[36] C. E. Johnston, E. D. Andrews, and J. Pitlick, "*In situ* determination of particle friction angles of fluvial gravels," Water Resour. Res. **34**, 2017–2030, doi:10.1029/98WR00312 (1998).
[37] T. Luckner, "Zum Bewegungsbeginn von Sedimenten," in *Institut für Wasserbau und Wasserwirtschaft* (Technische Universität Darmstadt, Darmstadt, Germany, 2002), p. 124.
[38] R. Fernandez Luque and R. van Beek, "Erosion and transport of bed-load sediment," J. Hydraul. Res. **14**, 127–144 (1976).
[39] Y. Chiew and G. Parker, "Incipient sediment motion on non-horizontal slopes," J. Hydraul. Res. **32**, 649–660 (1994).
[40] A. Armanini and C. Gregoretti, "Incipient sediment motion at high slopes in uniform flow condition," Water Resour. Res. **41**, W12431, doi:10.1029/2005WR004001 (2005).
[41] M. P. Lamb, W. E. Dietrich, and J. G. Venditti, "Is the critical Shields stress for incipient sediment motion dependent on channel-bed slope?," J. Geophys. Res. **113**, F02008, doi:10.1029/2007JF000831 (2008).
[42] J. R. D. Francis, "Experiments on the motion of solitary grains along the bed of a water-stream," Proc. R. Soc. London, Ser. A **332**, 443–471 (1973).
[43] J. E. Abbott and J. R. D. Francis, "Saltation and suspension trajectories of solid grains in a water stream," Philos. Trans. R. Soc. London, Ser. A **284**, 225–254 (1977).
[44] B. R. White and J. C. Schulz, "Magnus effect in saltation," J. Fluid Mech. **81**, 497–512 (1977).
[45] C. Ancey, T. Böhm, M. Jodeau, and P. Frey, "Statistical description of sediment transport experiments," Phys. Rev. E **74**, 011302 (2006).
[46] R. J. Munro, "The interaction of a vortex ring with a sloped sediment layer: Critical criteria for incipient grain motion," Phys. Fluids **24**, 026604 (2012).
[47] J. R. Agudo, S. Dasilva, and A. Wierschem, "How do neighbors affect incipient particle motion in laminar shear flow?," Phys. Fluids **26**, 053303 (2014).
[48] M. Amir, V. I. Nikora, and M. T. Stewart, "Pressure forces on sediment particles in turbulent open-channel flow: A laboratory study," J. Fluid Mech. **757**, 458–497 (2014).
[49] A. O. Celik, P. Diplas, and C. Dancey, "Instantaneous pressure measurements on a spherical grain under threshold flow conditions," J. Fluid Mech. **741**, 60–97 (2014).
[50] S. B. Pope, *Turbulent Flows* (Cambridge University Press, Cambridge, 2000).
[51] S.-I. Okazaki, "Some defects in Iwagaki's model for the criterion of sediment entrainment," Sci. Rep. Tohoku Univ., Ser. 7 **53**, 29–55 (2004).
[52] R. L. Miller and R. J. Byrne, "The angle of repose for a single grain on a fixed rough bed," Sedimentology **6**, 303–314 (1966).
[53] C. Ancey, F. Bigillon, P. Frey, and R. Ducret, "Rolling motion of a bead in a rapid water stream," Phys. Rev. E **67**, 011303 (2003).
[54] T. Loiseleux, P. Gondret, M. Rabaud, and D. Doppler, "Onset of erosion and avalanche for an inclined granular bed sheared by a continuous laminar flow," Phys. Fluids **17**, 103304 (2005).

[55] A. O. Celik, P. Diplas, C. L. Dancey, and M. Valyrakis, "Impulse and particle dislodgement under turbulent flow conditions," Phys. Fluids **22**, 046601 (2010).
[56] S. K. Bose and S. Dey, "Universal probability distributions of turbulence in open channel flows," J. Hydraul. Res. **48**, 388–394 (2010).
[57] S. Ikeda, "Some studies on the mechanics of bed load transport," Proc. Jpn. Soc. Civ. Eng. **185**, 61–69 (1971).
[58] A. J. Grass, "Structural features of turbulent flow over smooth and rough boundaries," J. Fluid Mech. **50**, 233–255 (1971).
[59] I. Nezu, "Turbulent structure in open channel flow," Ph.D. thesis, Kyoto University, Kyoto, 1977.
[60] I. Nezu and H. Nakagawa, *Turbulence in Open-Channel Flows* (Balkema, Rotterdam, The Netherlands, 1993).
[61] P. G. Saffman, "The lift on a small sphere in a slow shear flow," J. Fluid Mech. **22**, 385–400 (1965).
[62] P. G. Saffman, "Corrigendum, the lift on a small sphere in a slow shear flow," J. Fluid Mech. **31**, 624 (1968).
[63] W. S. Chepil, "The use of spheres to measure lift and drag on wind-eroded soil grains," Proc. Soil Sci. Soc. Am. **25**, 343–345 (1961).
[64] S. I. Rubinow and J. B. Keller, "The transverse force on a spinning sphere moving in a viscous fluid," J. Fluid Mech. **11**, 447–459 (1961).
[65] L. C. van Rijn, "Sediment transport. I. Bed load transport," J. Hydraul. Eng. **110**, 1431–1456 (1984).
[66] J. Rotta, "Das in Wändahe gültige Geschwindigkeitsgesetz turbulenter Strömungen," Archieve Appl. Mech. **18**, 277–280 (1950).
[67] J. Nikuradse, "Strömungsgesetze in rauhen Rohren," in *Research Bulletin* (Verein Deutscher Ingenieure, Forschungsheft, Berlin, Germany, 1933), Vol. 361, p. 22.
[68] ASCE Task Force, "Friction factor in open channels," J. Hydraul. Div., Am. Soc. Civ. Eng. **89**, 97–143 (1963).
[69] J. Best, S. Bennett, J. Bridge, and M. Leeder, "Turbulence modulation and particle velocities over flat sand beds at low transport rates," J. Hydraul. Eng. **123**, 1118–1129 (1997).
[70] S. Dey, S. Sarkar, and L. Solari, "Near-bed turbulence characteristics at the entrainment threshold of sediment beds," J. Hydraul. Eng. **137**, 945–958 (2011).
[71] S. Dey, R. Das, R. Gaudio, and S. K. Bose, "Turbulence in mobile-bed streams," Acta Geophys. **60**, 1547–1588 (2012).
[72] H. J. Casey, "Über Geschiebebewegung," in *Mitteilungen der Preussischen Versuchsanstalt für Wasserbau und Schiffbau* (Berlin, Germany, 1935).
[73] H. Kramer, "Sand mixtures and sand movement in fluvial model," Trans. ASCE **100**, 798–838 (1935).
[74] USWES, "Flume tests made to develop a synthetic sand which will not form ripples when used in movable bed models," Technical Memorandum 99-1, United States Waterways Experiment Station, Vicksburg, Mississippi, USA (1936).
[75] V. A. Vanoni, "Transportation of suspended sediment by water," Trans. ASCE **111**, 67–102 (1946).
[76] E. Meyer-Peter and R. Müller, "Formulas for bed-load transport," in *Proceedings of the 2nd Meeting of International Association for Hydraulic Research* (Stockholm, Sweden, 1948), Vol. 3, pp. 39–64.
[77] C. R. Neill, "Mean velocity criterion for scour of course uniform bed material," in *Proceedings of the 12th Congress of International Association for Hydraulic Research* (Fort Collins, Colorado, USA, 1967), Vol. 3, pp. 46–54.
[78] A. J. Grass, "Initial instability of fine bed sand," J. Hydraul. Div., Am. Soc. Civ. Eng. **96**, 619–632 (1970).
[79] S. J. White, "Plane bed thresholds of fine grained sediments," Nature (London) **228**, 152–153 (1970).
[80] E. Karahan, "Initiation of motion for uniform and non-uniform materials," Ph.D. thesis, Technical University, Istanbul, Turkey, 1975.
[81] P. Y. Julien, *Erosion and Sedimentation* (Cambridge University Press, 1995).
[82] R. L. Soulsby and R. J. S. Whitehouse, "Threshold of sediment motion in coastal environments," in *Proceedings of the Combined Australasian Coastal Engineering and Port Conference* (Christchurch, New Zealand, 1997), pp. 149–154.
[83] W. H. Hager and G. Del Giudice, "Discussion on movable bed roughness in alluvial rivers," J. Hydraul. Eng. **127**, 627–629 (2001).
[84] W. H. Hager and G. Oliveto, "Shields' entrainment criterion in bridge hydraulics," J. Hydraul. Eng. **128**, 538–542 (2002).
[85] S. Dey and R. V. Raikar, "Characteristics of loose rough boundary streams at near-threshold," J. Hydraul. Eng. **133**, 288–304 (2007).
[86] J. S. Fisher, B. L. Sill, and D. F. Clark, "Organic detritus particles: Initiation of motion criteria on sand and gravel beds," Water Resour. Res. **19**, 1627–1631, doi:10.1029/WR019i006p01627 (1983).